PROC. OF JSCE
No. 335, July 1983

EFFECTS OF SHEAR DEFORMATION AND ROTARY INERTIA ON SUSPENSION BRIDGE RESPONSE UNDER MOVING LOADS

*By Toshiro HAYASHIKAWA**

1. INTRODUCTION

Since the stiffness rigidity of suspension bridges is relatively small in comparison with other types of bridges, it makes dynamic behavior of suspension bridges under oscillations an important engineering problem. In designing this kind of bridge, therefore, it is required as an essential condition to determine accurately the natural frequencies and the mode shapes.

Thus far, a large number of papers has been published on free vertical vibration of suspension bridges[1)~5)] based on the deflection theory. This theory has become the established method of dynamic analysis of suspension bridges with any degree of accuracy, and has been used widely in their practical designs from an economical viewpoint. However, the effects of shear deformation and rotary inertia on suspension bridges have been neglected in the above literature in order to simplify the problems, since both effects are relatively small in comparison with those of bending deformation. In dynamic problems such as beams and frameworks, it is well known that the effect of shear deformation increases with increase of the ratio of cross-sectional dimensions to member length[6),7)]. The classical Bernoulli-Euler beam theory of flexural vibration has been recognized as inadequate for higher modes. Clough[8)] has described additional applications where higher modes of vibrations are important in engineering practice. In recent years, Abdel-Ghaffar and Housner[9)~11)] have developed a method of analyzing free vertical vibrations of suspension bridges by means of a digital computer and a finite element approach. They have reported the significant results of the comparison between the computed and measured natural frequencies and mode shapes. But, the consistency between the computations and measurements for the higher modes has been found to be less satisfactory. The source of disagreement in the results may be due to the simplifications introduced in the theory, such as neglecting the effects of shear deformation and rotary inertia of suspension bridges.

Some research work dealing with the dynamic response analysis of suspension bridges subjected to moving loads was made by using the modal analysis method[4),12)]. Hirai and Ito[13),14)] were the first to undertake large-scale experimental studies of railway suspension bridge models in the late 1960's. Their work is a source of much theoretical and experimental information on the problems discussed in this paper. To the writer's knowledge, no investigations have been made for dynamic behavior of moving loads across multi-span suspension bridges which take into account the effects of shear deformation and rotary inertia.

The primary objective of this study is to determine a sufficient number of natural frequencies and mode shapes, and to enable an accurate analysis from lower modes to higher modes of free vertically vibrating suspension bridges. The differential equations of motion of suspension bridges which take into account the effects of shear deformation and rotary inertia will be derived by applying Hamilton's principle. The secondary objective is to obtain a closed form solution for the dynamic response of multi-span suspension bridges traversed by moving loads with constant velocity, and to investigate the effects of shear deformation and rotary inertia on their dynamic response. Finally, a numerical example which uses data of actual long-span suspension bridge is presented to demonstrate the applicability of the dynamic analysis.

2. BASIC ASSUMPTIONS

The problem discussed herein is confined to the vertical vibration of suspension bridges. The conventional assumptions[1),2)] based on the deflection theory are used in the dynamic analysis under consideration of the effects of shear de-

* Member of JSCE, M. Eng., Research Associate, Dept. of Civil Eng., Hokkaido Univ.

formation and rotary inertia. Also, the following simplifications and additional assumptions are introduced:

(1) The additional horizontal component H_p of cable tension caused by inertia forces is small in comparison with the initial horizontal component H_w of cable tension due to dead loads.

(2) The types of stiffening girders of suspension bridges are grouped into two classes according to their structural characteristics. The hinged-span type bridge (two-hinged suspension bridge) is simply supported at the intermediate supports, as shown in **Fig. 1** (a); the continuous-span type bridge (continuous suspension bridge) is uninterruptedly supported over all spans, as shown in **Fig. 1** (b).

(3) The support conditions of the tower cable saddles are assumed to be as follows. The horizontal components H_p of cable tension are assumed to be the same on both sides of the tower in all spans of the cable (roller connection) as shown in **Fig. 2** (a). This presupposes that the tower cable saddles are free to move horizontally upon roller nests and that there is no tower resistance to displacement at the top. Next, the horizontal components $H_{p,i}$ of cable tension on both sides of the tower may differ slightly from the friction forces at the tower cable saddles

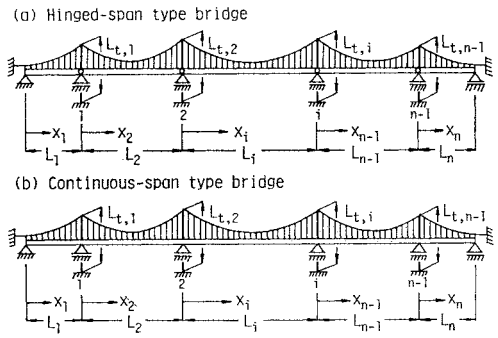

Fig. 1 Geometry and Coordinate System of Multispan Suspension Bridge with Different Types of Stiffening Girders.

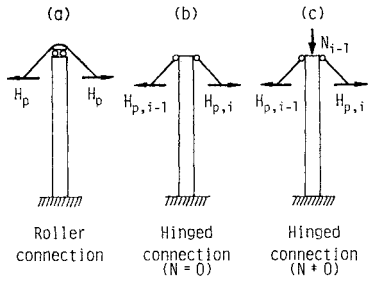

Fig. 2 Support Conditions of Tower Cable Saddles.

(hinged connection). Then, the effect of the elasticity of towers is considered in the dynamic analysis of suspension bridges. **Figs. 2** (b) and 2(c) show the cases of neglecting and considering the effect of an axial force N_i acting on the top of the tower, respectively.

(4) In the dynamic response analysis of suspension bridges under moving loads, the effects of the damping force and the mass associated with the moving load are neglected.

(5) The bridge is traversed by a constant concentrated load moving from left to right at a constant velocity. At time $t=0$, the moving load arrives at the end of the first span and the dynamic response of the bridge starts at that time from rest condition.

3. FREE VERTICAL VIBRATION ANALYSIS

(1) Differential Equations of Motion

The differential equations of motion of a suspension bridge taking into account the effects of shear deformation and rotary inertia, and the associated boundary conditions will be derived by means of Hamilton's principle[15]. In the Timoshenko beam theory, the kinetic energy T of the vertically vibrating bridge due to translation and rotation is expressed

$$T=\frac{1}{2}\sum_{i=1}^{n}\int_0^{L_i}\frac{w_i}{g}\left(\frac{\partial\eta_i}{\partial t}\right)^2 dx_i + \frac{1}{2}\sum_{i=1}^{n}\int_0^{L_i}J_i\left(\frac{\partial\theta_i}{\partial t}\right)^2 dx_i \quad \cdots\cdots(1)$$

where n is the number of spans, L_i is the length of the ith span, w_i is the dead load of the stiffening girder or truss (w_{gi}) per unit length of the ith span plus the dead weight of the cable (w_c) per unit length, η_i is the vertical vibrational displacement at distance x_i from the left end and at time t, θ_i is the bending slope, g is the acceleration of gravity, and J_i is the mass moment of inertia per unit length of the ith stiffening girder about the neutral axis. J_i is related to the moment of inertia of the ith stiffening girder (I_i) by

$$J_i=\rho_{gi}I_i=\frac{w_{gi}I_i}{gA_i}$$

where ρ_{gi} is the mass density of the ith stiffening girder, and A_i is the reduced area of the ith stiffening girder (upper and lower chord members, and diagonal and vertical truss members). The total slope of the deflection curve at point x_i can be expressed as

$$\partial\eta_i/\partial x_i=\theta_i+\beta_i \quad \cdots\cdots(2)$$

where β_i is the shearing slope at the neutral axis in the same cross section. Next, the potential energy V_g of the stiffening girder due to the

effects of bending and shearing deformation can be expressed by

$$V_g=\frac{1}{2}\sum_{i=1}^{n}\int_0^{L_i}E_iI_i\left(\frac{\partial\theta_i}{\partial x_i}\right)^2dx_i+\frac{1}{2}\sum_{i=1}^{n}\int_0^{L_i}k_iA_iG_i\left(\frac{\partial\eta_i}{\partial x_i}-\theta_i\right)^2dx_i \quad \cdots(3)$$

where E_i and G_i are Young's modulus and the shear modulus of the stiffening girder, respectively, and k_i is the shear coefficient[16]. Finally, the potential energy V_c of the cable may be written as[1),11)]

$$V_c=\frac{1}{2}\sum_{i=1}^{n}\int_0^{L_i}H_w\left(\frac{\partial\eta_i}{\partial x_i}\right)^2dx_i+\frac{1}{2}\sum_{i=1}^{n}\frac{L_cH_{p,i}^2}{E_cA_c} \quad \cdots(4)$$

where E_c and A_c are Young's modulus and the cross-sectional area of the cable, respectively, and L_c is the virtual length defined by the following equation

$$L_c=\sum_{i=1}^{n}L_{c,i} \text{ and } L_{c,i}=\int_0^{L_i}\left(\frac{ds_i}{dx_i}\right)^3dx_i \quad \cdots(5)$$

where ds_i is a differential element along the cable curve. This integral extends over the entire length of cable. The relationship between η_i and $H_{p,i}$ is expressed by the so-called cable equation of compatibility that relates the elastic stretching of the cable to the geometric displacement, as follows:

(1) In the case of the roller connection as shown in **Fig. 2**(a), the cable equation is

$$\frac{L_c}{E_cA_c}H_p-\sum_{i=1}^{n}\frac{w_i}{H_w}\int_0^{L_i}\eta_i\,dx_i=0 \quad \cdots(6)$$

(2) In the case of the hinged connection as shown in **Figs. 2**(b) and 2(c), the cable equations on the ith span of suspension bridges are given[5),17)]

$$\left.\begin{aligned}&\frac{L_{c,i}}{E_cA_c}H_{p,i}-\frac{w_i}{H_w}\int_0^{L_i}\eta_i\,dx_i=-\delta_i^l+\delta_i^r\\&\text{for}\quad i=1,2,\cdots,n\end{aligned}\right\}\cdots(7)$$

where δ_i^l and δ_i^r are the horizontal displacements of the tower top at the left and right end supports of the ith span of suspension bridges, respectively. In the case of **Fig. 2**(b), the horizontal forces are acting only on the top of the tower and these displacements can be written as

$$\left.\begin{aligned}\delta_i^l&=-\frac{L_{t,i-1}^3}{3E_tI_{t,i-1}}(H_{p,i-1}-H_{p,i})\\\delta_i^r&=-\frac{L_{t,i}^3}{3E_tI_{t,i}}(H_{p,i}-H_{p,i+1})\end{aligned}\right\}\cdots\cdots(8\cdot a,b)$$

where $E_tI_{t,i}$ and $L_{t,i}$ are the average flexural stiffness and the height of the ith tower, respectively. In the case of **Fig. 2**(c), both the axial and horizontal forces are acting on the top of the tower and these displacements can be written as

$$\delta_i^l=-\frac{L_{t,i-1}}{N_{i-1}}\left\{\frac{\tan(K_{i-1}L_{t,i-1})}{K_{i-1}L_{t,i-1}}-1\right\}\times(H_{p,i-1}-H_{p,i}),$$

$$\delta_i^r=-\frac{L_{t,i}}{N_i}\left\{\frac{\tan(K_iL_{t,i})}{K_iL_{t,i}}-1\right\}(H_{p,i}-H_{p,i+1}) \quad \cdots\cdots(9\cdot a,b)$$

where $K_i=\sqrt{N_i/(E_tL_{t,i})}$.

The governing equations of motion of the suspension bridge including the effects of shear deformation and rotary inertia, will be derived by applying Hamilton's principle

$$\int_{t_1}^{t_2}\delta\{T-(V_g+V_c)\}dt=0 \quad \cdots\cdots(10)$$

where δ is the variational operator taken during the indicated time interval. Substituting Eqs. (1), (3), and (4) into Eq. (10) for integration and taking variations, the following differential equations of motion are obtained

$$E_iI_i\frac{\partial^2\theta_i}{\partial x_i^2}+k_iA_iG_i\left(\frac{\partial\eta_i}{\partial x_i}-\theta_i\right)-\frac{w_{gi}I_i}{gA_i}\frac{\partial^2\theta_i}{\partial t^2}=0 \quad \cdots\cdots(11)$$

$$k_iA_iG_i\left(\frac{\partial^2\eta_i}{\partial x_i^2}-\frac{\partial\theta_i}{\partial x_i}\right)+(H_w+H_{p,i})\frac{\partial^2\eta_i}{\partial x_i^2}-\frac{w_i}{H_w}H_{p,i}-\frac{w_i}{g}\frac{\partial^2\eta_i}{\partial t^2}=0 \quad \cdots\cdots(12)$$

(2) Eigenfunctions

By eliminating θ_i from Eqs. (11) and (12), and neglecting the differential of high order included the term $H_w+H_{p,i}$, the following equation may be obtained

$$E_iI_i\frac{\partial^4\eta_i}{\partial x_i^4}-\left(\frac{w_{gi}I_i}{gA_i}+\frac{w_iE_iI_i}{gk_iA_iG_i}\right)\frac{\partial^4\eta_i}{\partial x_i^2\partial t^2}+\frac{w_{gi}w_iI_i}{g^2k_iA_i^2G_i}\frac{\partial^4\eta_i}{\partial t^4}-(H_w+H_{p,i})\frac{\partial^2\eta_i}{\partial x_i^2}+\frac{w_i}{H_w}H_{p,i}+\frac{w_i}{g}\frac{\partial^2\eta_i}{\partial t^2}=0$$

The terms of dead loads w_i and w_{gi} are included very complicated in the above equation. Here, it is assumed to obtain eigenfunctions of a suspension bridge that $H_w\fallingdotseq H_w+H_{p,i}$ and $w_i\fallingdotseq w_{gi}$. A more complete differential equation for the vertically vibrating suspension bridge can be written as follows

$$E_iI_i\frac{\partial^4\eta_i}{\partial x_i^4}-\frac{w_i}{g}\left(\frac{I_i}{A_i}+\frac{E_iI_i}{k_iA_iG_i}\right)\frac{\partial^4\eta_i}{\partial x_i^2\partial t^2}+\frac{w_i^2I_i}{g^2k_iA_i^2G_i}\frac{\partial^4\eta_i}{\partial t^4}-H_w\frac{\partial^2\eta_i}{\partial x_i^2}+\frac{w_i}{H_w}H_{p,i}+\frac{w_i}{g}\frac{\partial^2\eta_i}{\partial t^2}=0 \quad \cdots\cdots(13)$$

Table 1 List of Eigenfunctions for Suspension Bridge Including Effects of Shear Deformation and Rotary Inertia.

Conditions	Eigenfunctions $V_i(x_i)$ and $\Theta_i(x_i)$	Values of μ_i and ν_i	Values of $R_{\mu i}$ and $R_{\nu i}$
$b_i^2(r_i^2+s_i^2)\leq c_i^2$	$V_i(x_i)=A_i\cos\frac{\mu_i x_i}{L_i}+B_i\sin\frac{\mu_i x_i}{L_i}+C_i\cosh\frac{\nu_i x_i}{L_i}+D_i\sinh\frac{\nu_i x_i}{L_i}+\frac{g}{\omega^2 H_w}H_{p,i}$	$\mu_i=\sqrt{W_i(Z_i-1)}$	$R_{\mu i}=\frac{b_i^2 s_i^2-\mu_i^2(1+c_i^2 s_i^2)}{\mu_i L_i}$
	$\Theta_i(x_i)=R_{\mu i}\left(A_i\sin\frac{\mu_i x_i}{L_i}-B_i\cos\frac{\mu_i x_i}{L_i}\right)+R_{\nu i}\left(C_i\sinh\frac{\nu_i x_i}{L_i}+D_i\cosh\frac{\nu_i x_i}{L_i}\right)$	$\nu_i=\sqrt{W_i(Z_i+1)}$	$R_{\nu i}=\frac{b_i^2 s_i^2+\nu_i^2(1+c_i^2 s_i^2)}{\nu_i L_i}$
$b_i^2(r_i^2+s_i^2)>c_i^2$ and $b_i^2 r_i^2 s_i^2\leq 1$	$V_i(x_i)=A_i\cos\frac{\mu_i x_i}{L_i}+B_i\sin\frac{\mu_i x_i}{L_i}+C_i\cosh\frac{\nu_i x_i}{L_i}+D_i\sinh\frac{\nu_i x_i}{L_i}+\frac{g}{\omega^2 H_w}H_{p,i}$	$\mu_i=\sqrt{-W_i(Z_i+1)}$	$R_{\mu i}=\frac{b_i^2 s_i^2-\mu_i^2(1+c_i^2 s_i^2)}{\mu_i L_i}$
	$\Theta_i(x_i)=R_{\mu i}\left(A_i\sin\frac{\mu_i x_i}{L_i}-B_i\cos\frac{\mu_i x_i}{L_i}\right)+R_{\nu i}\left(C_i\sinh\frac{\nu_i x_i}{L_i}+D_i\cosh\frac{\nu_i x_i}{L_i}\right)$	$\nu_i=\sqrt{-W_i(Z_i-1)}$	$R_{\nu i}=\frac{b_i^2 s_i^2+\nu_i^2(1+c_i^2 s_i^2)}{\nu_i L_i}$
$b_i^2(r_i^2+s_i^2)>c_i^2$ and $b_i^2 r_i^2 s_i^2>1$	$V_i(x_i)=A_i\cos\frac{\mu_i x_i}{L_i}+B_i\sin\frac{\mu_i x_i}{L_i}+C_i\cos\frac{\nu_i x_i}{L_i}+D_i\sin\frac{\nu_i x_i}{L_i}+\frac{g}{\omega^2 H_w}H_{p,i}$	$\mu_i=\sqrt{-W_i(1-Z_i)}$	$R_{\mu i}=\frac{b_i^2 s_i^2-\mu_i^2(1+c_i^2 s_i^2)}{\mu_i L_i}$
	$\Theta_i(x_i)=R_{\mu i}\left(A_i\sin\frac{\mu_i x_i}{L_i}-B_i\cos\frac{\mu_i x_i}{L_i}\right)+R_{\nu i}\left(C_i\sin\frac{\nu_i x_i}{L_i}-D_i\cos\frac{\nu_i x_i}{L_i}\right)$	$\nu_i=\sqrt{-W_i(1+Z_i)}$	$R_{\nu i}=\frac{b_i^2 s_i^2-\nu_i^2(1+c_i^2 s_i^2)}{\nu_i L_i}$

Note: A_i, B_i, C_i, and D_i are integration constants, $W_i=\{c_i^2-b_i^2(r_i^2+s_i^2)\}/2$, and $Z_i=\sqrt{1+\{4b_i^2(1-b_i^2r_i^2s_i^2)\}/\{c_i^2-b_i^2(r_i^2+s_i^2)\}^2}$ and $i=1, 2, 3, \cdots, n$.

In this manner, the effects of shear deformation and rotary inertia are represented by the second and third terms of Eq. (13). By writing the solutions of Eq. (13) in the well-known form

$$\left.\begin{aligned}\eta_i&=V_i(x_i)\exp(j\omega t)\,,\\ \theta_i&=\Theta_i(x_i)\exp(j\omega t)\,,\\ H_{p,i}&=H_{p,i}\exp(j\omega t)\end{aligned}\right\}\quad\cdots\cdots\cdots\cdots(14\cdot a\sim c)$$

where

$$\left.\begin{aligned}V_i(x_i)&=\exp(\lambda_i x_i/L_i)\,,\\ \Theta_i(x_i)&=\exp(\lambda_i x_i/L_i)\end{aligned}\right\}\quad\cdots\cdots\cdots\cdots(15\cdot a,b)$$

and $j=\sqrt{-1}$, ω is the natural circular frequency of the suspension bridge, and λ_i is the undetermined parameter. The following characteristic equation is obtained by substituting Eqs. (14) and (15) into Eq. (13)

$$\lambda_i^4+\{b_i^2(r_i^2+s_i^2)-c_i^2\}\lambda_i^2-b_i^2(1-b_i^2r_i^2s_i^2)=0\quad\cdots(16)$$

where

$$\left.\begin{aligned}b_i^2&=\frac{w_i L_i^4\omega^2}{gE_iI_i}\qquad c_i^2=\frac{H_w L_i^2}{E_iI_i}\,,\\ r_i^2&=\frac{I_i}{A_iL_i^2}\,,\qquad s_i^2=\frac{E_iI_i}{k_iA_iG_iL_i^2}\end{aligned}\right\}\quad\cdots\cdots(17\cdot a\sim d)$$

The general solution [eigenfunction $V_i(x_i)$] of Eq. (13) can be obtained by using trigonometric and hyperbolic functions as shown in **Table 1**. Also, the other eigenfunction $\Theta_i(x_i)$ is related the eigenfunction $V_i(x_i)$ by either Eq. (11) or Eq. (12), and the results are summarized in the same **Table 1**.

The property of orthogonality of the eigenfunctions $V_i(x_i)$ and $\Theta_i(x_i)$ can be obtained by using Rayleigh's method[18),19)]. Thus the formulation of the orthogonality relationship for the natural modes of free vibration is written as follows

$$\sum_{i=1}^{n}\int_0^{L_i}\left\{V_{mi}(x_i)V'_{m'i}(x_i)+\frac{I_i}{A_i}\Theta_{mi}(x_i)\Theta'_{m'i}(x_i)\right\}\times dx_i=0\quad\text{for } m\neq m'\quad\cdots\cdots\cdots\cdots(18)$$

where m and m' represent the natural mode orders, and are different from each other.

(3) Boundary Conditions and Frequency Equation

The natural and geometrical boundary conditions for vertically vibrating suspension bridges are derived as follows

$$E_iI_i\frac{\partial\theta_i}{\partial x_i}=0\quad\text{or}\quad\theta_i=0\,,$$

and

$$k_iA_iG_i\left(\frac{\partial\eta_i}{\partial x_i}-\theta_i\right)+H_w\frac{\partial\eta_i}{\partial x_i}+H_{p,i}\frac{dy_i}{dx_i}=0$$

or $\eta_i=0$,

at $x_i=0$ and $x_i=L_i$ for $i=1, 2, \cdots, n$

$$\cdots\cdots\cdots\cdots(19\cdot a,b)$$

where y_i is the ordinate of the cable parabola. The first parts of Eqs. (19·a) and (19·b) represent the bending moment and shearing force at each end of the stiffening girders, respectively.

The eigenfunctions $V_i(x_i)$ and $\Theta_i(x_i)$ in **Table 1** involve two unknown quantities with respect to the natural circular frequency ω and the additional cable tension $H_{p,i}$. These unknown quantities are determined by both the boundary conditions at the supports of the stiffening girder and the cable equations. By substituting the eigenfunctions $V_i(x_i)$ and $\Theta_i(x_i)$ into the equations of the above-mentioned boundary conditions, the following matrix notation is ob-

tained[5),17)]

$$\boldsymbol{Aa}=\boldsymbol{Hh} \quad \cdots\cdots(20)$$

where

$$\boldsymbol{a}=\{A_1, B_1, C_1, D_1, A_2, B_2, C_2, D_2, \cdots, A_n, B_n, C_n, D_n\}^T,$$

$$\boldsymbol{h}=\{H_{p,1}, H_{p,2}, \cdots, H_{p,n}\}^T \quad \cdots\cdots(21\cdot a,b)$$

The orders of the coefficient matrices $\boldsymbol{A}$ and $\boldsymbol{H}$ are $4n\times 4n$ and $4n\times n$, respectively. Next, the cable equations expressing the relationship between the vertical displacements and the cable tensions are used to determine the natural circular frequency. The relation between the vectors $\boldsymbol{a}$ and $\boldsymbol{h}$ is also obtained by substituting the eigenfunction $V_i(x_i)$ into either Eq. (6) or Eq. (7)

$$\boldsymbol{Ga}=\boldsymbol{Eh} \quad \cdots\cdots(22)$$

The coefficient matrices $\boldsymbol{G}$ and $\boldsymbol{E}$ are of the orders $n\times 4n$ and $n\times n$, respectively. In the above Eqs. (20) and (22), it should be noted that the order of the vector $\boldsymbol{h}$ is 1×1 in the case of the roller connection because the unknown constant H_p in Eq. (6) is only a term throughout each span.

The homogeneous equation on the vector $\boldsymbol{a}$ is obtained by eliminating the vector $\boldsymbol{h}$ from Eqs. (20) and (22)

$$(\boldsymbol{A}-\boldsymbol{HE}^{-1}\boldsymbol{G})\boldsymbol{a}=\boldsymbol{0} \quad \cdots\cdots(23)$$

A nontrivial solution of Eq. (23) is possible only when the determinant of the matrix of order $4n\times 4n$ vanishes

$$\det|\boldsymbol{A}-\boldsymbol{HE}^{-1}\boldsymbol{G}|=0 \quad \cdots\cdots(24)$$

This equation is called the frequency equation, and is a transcendental equation on the natural circular frequencies (eigenvalues, ω). The roots may be solved by applying the Regula-Falsi method[20)] and by using a high-speed digital computer. Finally, the relative values of the constants in the vectors $\boldsymbol{a}$ and $\boldsymbol{h}$ can be determined by Eqs. (23) and (22), respectively.

4. SERIES EXPANSION OF LOADS

The external distributed loads $p(x)$ and moments $m(x)$ may be represented by the following linear series of the eigenfunctions $V_i(x_i)$ and $\Theta_i(x_i)$[19)]

$$p_s(x_s)\frac{g}{w_s A_s}=\sum_{m=1}^{\infty} q_{ms} V_{ms}(x_s) \quad \cdots\cdots(25)$$

$$m_s(x_s)\frac{g}{w_s I_s}=\sum_{m=1}^{\infty} q_{ms}\Theta_{ms}(x_s) \quad \cdots\cdots(26)$$

where the subscript, s, indicates the span number of the applied loads and moments, and q_{ms} represents the unknown coefficient. Multiplying both sides of Eq. (25) by $V'_{mi}(x_i)$ and of Eq. (26) by $\Theta'_{mi}(x_i)$, adding and integrating the result over the span length, in view of Eq. (18)

$$q_{ms}=\frac{g}{w_s M_m^2}\int_0^{L_s}\{p_s(x_s)V_{ms}(x_s)+m_s(x_s)\Theta_{ms}(x_s)\}dx_s \quad \cdots\cdots(27)$$

and

$$M_m^2=\sum_{i=1}^{n}\int_0^{L_i}\left\{V_{mi}^2(x_i)+\frac{I_i}{A_i}\Theta_{mi}^2(x_i)\right\}dx_i \quad \cdots\cdots(28)$$

Consequently, the coefficients q_{ms} of Eqs. (25) and (26) are determined by integrating Eq. (27), when the concrete functions $p_s(x_s)$ and $m_s(x_s)$ are given. **Table 2** contains some sample results of the coefficients q_{ms} for loading conditions as shown in **Figs. 3** and **4**. The other loading types are obtained by means of the superposition of fundamental loading conditions shown in **Table 2**.

Table 2 Types of Loading Conditions and Coefficients q_{ms}.

Types of load and moment	Coefficients, q_{ms}
Partial uniform load (**Fig. 3**)	$q_{ms}=\frac{2gp_sL_s}{w_sM_m^2}\left\{\left(\frac{1}{\mu_{ms}}\right)\sin\frac{\mu_{ms}\varepsilon_s}{L_s}\left(A_{ms}\cos\frac{\mu_{ms}a_s}{L_s}+B_{ms}\sin\frac{\mu_{ms}a_s}{L_s}\right)+\left(\frac{1}{\nu_{ms}}\right)\sinh\frac{\nu_{ms}\varepsilon_s}{L_s}\left(C_{ms}\cosh\frac{\nu_{ms}a_s}{L_s}+D_{ms}\sinh\frac{\nu_{ms}a_s}{L_s}\right)+\frac{gH_{p,s}\varepsilon_s}{\omega_m^2HwL_s}\right\}$
Partial uniform monent (**Fig. 3**)	$q_{ms}=\frac{2gm_sL_s}{w_sM_m^2}\left\{\left(\frac{R_{m,s}}{\mu_{ms}}\right)\sin\frac{\mu_{ms}\varepsilon_s}{L_s}\left(A_{ms}\sin\frac{\mu_{ms}a_s}{L_s}-B_{ms}\cos\frac{\mu_{ms}a_s}{L_s}\right)+\left(\frac{R_{m,s}}{\nu_{ms}}\right)\sinh\frac{\nu_{ms}\varepsilon_s}{L_s}\left(C_{ms}\sinh\frac{\nu_{ms}a_s}{L_s}+D_{ms}\cosh\frac{\nu_{ms}a_s}{L_s}\right)\right\}$
Concentrated load (**Fig. 4**)	$q_{ms}=\frac{gP_s}{w_sM_m^2}V_{ms}(a_s)$
Concentrated moment (**Fig. 4**)	$q_{ms}=\frac{gM_s}{w_sM_m^2}\Theta_{ms}(a_s)$

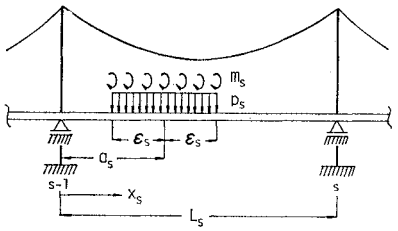

Fig. 3 External Partial Uniform Load p_s and Moment m_s.

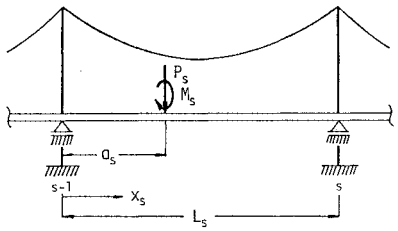

Fig. 4 External Concentrated Load P_s and Moment M_s.

5. DYNAMIC RESPONSE ANALYSIS

The modal analysis method is used here to solve the problem of forced vibration of suspension bridges under moving loads. When the moving load is passing through the sth span of the bridge, the dynamic deflection $\eta(x_r, t_s)$ can be expressed by the following equation

$$\eta(x_r, t_s)=\sum_{m=1}^{\infty} V_{mr}(x_r)q_{ms}(t_s) \quad \cdots\cdots(29)$$

where the subscript, r, represents the measuring span number, and $q_{ms}(t_s)$ is the function of time t_s. The equation of motion for elastic structures is given

$$\ddot{q}_{ms}(t_s)+\omega_m^2 q_{ms}(t_s)=Q_{ms}(t_s) \quad \cdots\cdots(30)$$

where a dot denotes the differentiation with respect to time, and $Q_{ms}(t_s)$ is the external force. When the concentrated load P moves at a constant velocity v on the sth span, the external force $Q_{ms}(t_s)$ is determined by substituting $a_s=vt_s$ into the equation in **Table 2**

$$Q_{ms}(t_s)=\frac{gP}{w_s M_m^2}V_{ms}(vt_s) \quad \cdots\cdots(31)$$

The solution of Eq. (30) is obtained by using Duhamel's integral as follows

$$q_{ms}(t_s)=\frac{gP}{w_s\omega_m M_m^2}\int_0^{t_s} V_{ms}(v\tau)\sin\omega_m(t_s-\tau)d\tau + q_{ms}(0)\cos\omega_m t_s+\dot{q}_{ms}(0)/\omega_m \sin\omega_m t_s \quad \cdots\cdots(32)$$

where $q_{ms}(0)$ and $\dot{q}_{ms}(0)$ are the integration constants, and are determined by initial conditions at time $t_s=0$. The dynamic response analysis discussed herein is considered for multispan suspension bridges as shown in **Figs. 1** (a) and **1** (b). When the moving load traverses the second span and subsequent spans, therefore, the initial conditions for each span are necessary to decide the constants $q_{ms}(0)$ and $\dot{q}_{ms}(0)$. Since the procedure for determining the above constants is explained in references 17) and 19), it is not explained here due to limited space.

6. NUMERICAL RESULTS

A numerical example is presented to demonstrate the effectiveness of the analytical method developed here and to investigate the dynamic behavior of suspension bridges. Computations using data from the Innoshima Suspension Bridge located between Honshu and Shikoku in Japan provide the basis for this example. The geometry of the bridge and the structure properties are given as follows:

(1) Stiffening girder, $L_1=L_3=250$ m, $L_2=770$ m, $w_1=w_3=21.09$ t/m (207 kN/m), $w_2=20.31$ t/m (199 kN/m), $I_1=I_3=4.216$ m^4, $I_2=4.904$ m^4, $A_1=A_3=0.2082$ m^2, $A_2=0.2422$ m^2, $E=2.1\times10^7$ t/m^2 (206 GPa), and $G=8.1\times10^6$ t/m^2 (80 GPa).

(2) Cable, cable sag length in main span $f=76$ m, $A_c=0.4562$ m^2, $H_w=19{,}806$ t (194 MN), and $E_c=2.0\times10^7$ t/m^2 (196 GPa).

(3) Tower, $L_{t,1}=L_{t,2}=138.85$ m, $I_{t,1}=I_{t,2}=6.640$ m^4, and $E_t=2.1\times10^7$ t/m^2 (206 GPa).

(1) Natural Frequencies

It is observed that the dimensionless parameters b_i, c_i, r_i, and s_i shown in Eq. (17) correspond to the effects of bending deformation, axial tensile force, rotary inertia, and shear deformation, respectively. Here, it is seen from these parameters that the most suitable parameters to investigate the effects of shear deformation and rotary inertia on the dynamic characteristics of suspension bridges are $r=\sqrt{I/(AL^2)}$ and $\pi=kG/E$.

The eigenvalue problem resulting from Eq. (24) has been solved on a high-speed digital computer. The computed natural periods are shown in **Table 3** for the first five modes of asymmetric and symmetric vibrations. In the lower modes, there is an imperceptible difference between the roller connection and the hinged connection, while in the higher modes, there is almost no recognizable difference in the cable support conditions as shown in **Fig. 2**. Also, there is a considerable difference between the hinged-span type and the continuous-span type bridges in both asymmetric and symmetric

Table 3 Computed Natural Periods (In Seconds) of Vertical Vibration of Innoshima Suspension Bridge ($r=0.01$, $\pi=0.2$).

Mode types of vertical vibration	Mode order	Hinged-span type			Continuous-span type		
		Roller connection	Hinged connection ($N=0$)	Hinged connection ($N\neq 0$)	Roller connection	Hinged connection ($N=0$)	Hinged connection ($N\neq 0$)
Asymmetric mode	1st	6.8640	6.8640	6.8640	6.3763	6.3746	6.3755
	2nd	4.0821	4.0671	4.0754	3.6319	3.6214	3.6267
	3rd	2.6645	2.6645	2.6645	2.4661	2.4660	2.4660
	4th	1.4206	1.4206	1.4206	1.4333	1.4333	1.4333
	5th	0.8981	0.8981	0.8981	1.2757	1.2757	1.2757
Symmetric mode	1st	6.0397	6.0169	6.0295	5.7487	5.7280	5.7395
	2nd	4.0431	4.0411	4.0422	3.9814	3.9799	3.9807
	3rd	2.8013	2.8012	2.8013	2.6314	2.6313	2.6314
	4th	1.8830	1.8830	1.8830	1.7909	1.7909	1.7909
	5th	1.1103	1.1103	1.1103	1.3451	1.3451	1.3451

modes. The values of the natural periods of two-hinged suspension bridges are generally larger than those of continuous suspension bridges.

In order to show the effects of shear deformation and rotary inertia on the natural frequencies of the suspension bridge, the results of the ratio of natural frequencies ω^*/ω are used in this paper. Here, ω^* is the frequency due to Timoshenko beam theory including both shear deformation and rotary inertia, and ω is the frequency due to Bernoulli-Euler beam theory including only bending deformation. The results of ω^*/ω versus r for the first five modes, with the range of r from 0.002 to 0.05, are shown in **Figs. 5, 6,** and **7** for the parameter $\pi=0.1$, 0.2, and 0.4, respectively. It is seen that the reduction of the ratio of natural frequencies increases by increasing the values of r and by decreasing the values of π (i.e., as the shear coefficient k_i decreases). It is also observed from the curves shown in these figures that the effects of shear deformation and rotary inertia become quite pronounced for higher modes of both asymmetric and symmetric vibrations. For the first principal modes, the reduction of the curves of continuous suspension bridges is larger than that of hinged suspension bridges. Namely, the effects of shear deformation and rotary inertia on continuous suspension bridges are of great dimensions in

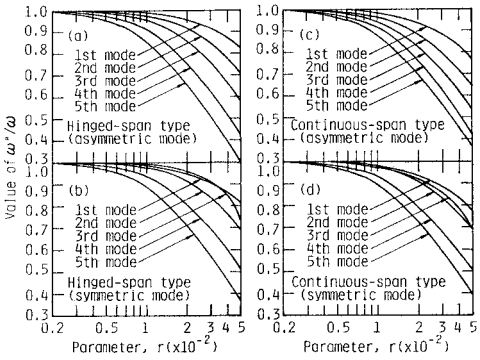

Fig. 6 Effects of Shear Deformation and Rotary Inertia on Computed Natural Frequencies ($\pi=0.2$).

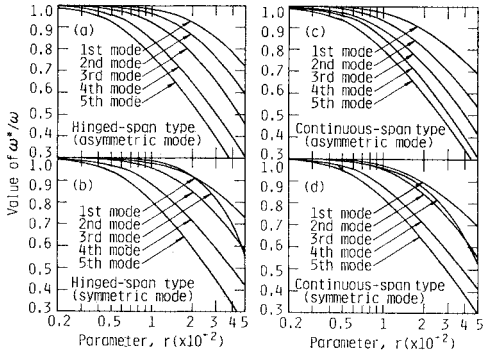

Fig. 5 Effects of Shear Deformation and Rotary Inertia on Computed Natural Frequencies ($\pi=0.1$).

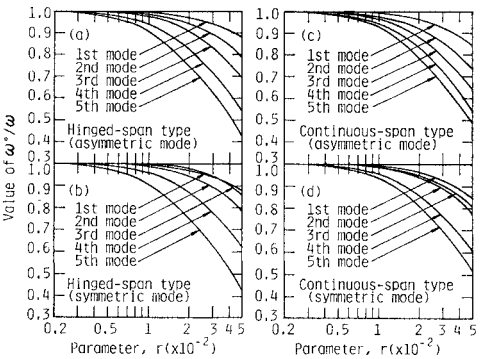

Fig. 7 Effects of Shear Deformation and Rotary Inertia on Computed Natural Frequencies ($\pi=0.4$).

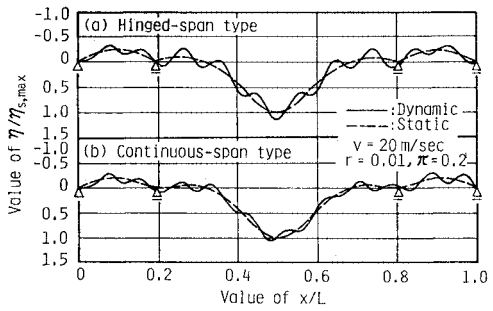

Fig. 8 History Curves of Deflection at Center Point of Second Span.

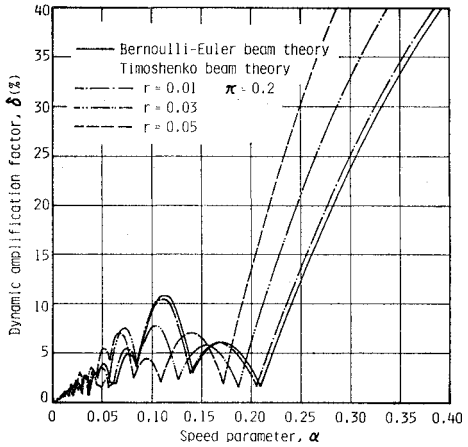

Fig. 9 δ–α Relation Diagram for Deflection at Center Point of First Span (Hinged-Span Type Bridge).

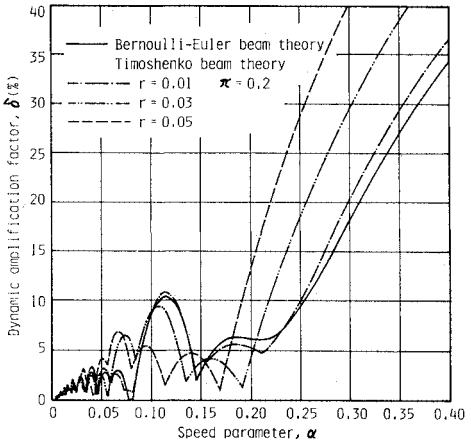

Fig. 10 δ–α Relation Diagram for Deflection at Center Point of First Span (Continuous-Span Type Bridge).

comparison with those on hinged suspension bridges.

(2) History Curves

Fig. 8 shows that response history curves of deflection of the suspension bridge, when a concentrated load with a constant velocity v 20 m/s is passing from left to right. The abscissa in this figure represents the distance between the left support and the position of the load on the bridge normalized with respect to the total bridge length. The ordinate of the history curve is normalized with respect to the maximum static response value of the measuring point under consideration. Also, the static response is shown in the broken line, and that is the response if the speed of the moving load approaches zero. These numerical computations are carried out using up to 12 terms of the series of Eq. (29). Although the static response of the hinged-span type bridge produces the bent-angle at the intermediate supports, there is no bent-angle in the static response of the continuous-span type bridge.

The dynamic effect is evaluated by the following equation[19]

$$\delta=(\eta_{d,\max}-\eta_{s,\max})/\eta_{s,\max}\times 100 \quad \cdots\cdots(33)$$

(as a percentage)

where δ is the dynamic amplification factor, and $\eta_{d,\max}$ and $\eta_{s,\max}$ are the maximum values of the dynamic and static response, respectively. It is seen from **Figs. 8**(a) and **8**(b) that the dynamic amplification factors calculated by Eq. (33) are 19.92% and 10.66%, respectively.

(3) Dynamic Amplification Factors

The speed parameter α defined by the following equation is used to investigate the dynamic characteristics of suspension bridges under moving loads

$$\alpha=\mu_{1r}v/\omega_1 \quad \cdots\cdots(34)$$

where ω_1 is the fundamental natural circular frequency. The relation between the dynamic amplification factor and the speed parameter are shown in **Figs. 9**~**12**. The δ–α relation diagrams for the range of values of the speed parameter $0\leqq\alpha\leqq 0.40$ are calculated by increasing in increments of 0.0025.

The diagrams of the dynamic amplification factor have a number of local peaks and show a tendency to increase as the speed parameter increases. Also, the dynamic amplification factors tend to increase wholly by increasing the parameter r. The effects of shear deformation and rotary inertia are obvious upon comparing the curves as shown in **Figs. 9** and **10**, when the measuring point is the center point of the first

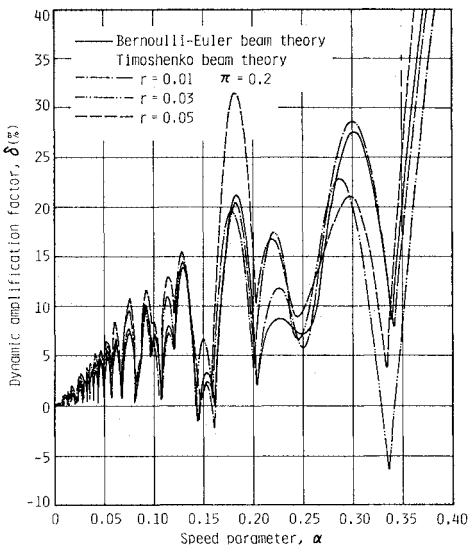

Fig. 11 δ–α Relation Diagram for Deflection at Center Point of Second Span (Hinged-Span Type Bridge).

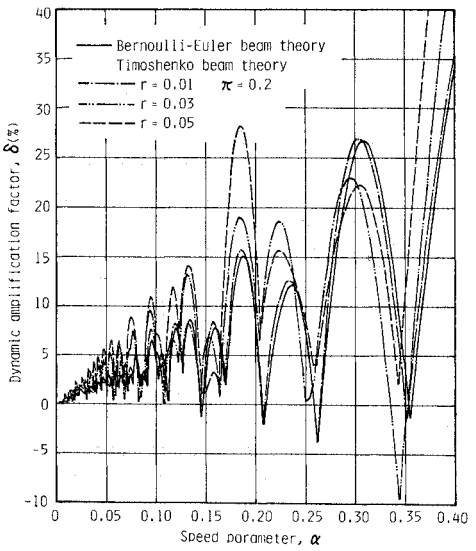

Fig. 12 δ–α Relation Diagram for Deflection at Center Point of Second Span (Continuous-Span Type Bridge).

span and the speed parameter α is larger than 0.20. The great effects of shear deformation and rotary inertia on dynamic response are observed in suspension bridges with the continuous stiffening girder. The diagrams of the second span are, for the range of α considered, very complicated in comparison with those of the first span. This result is interpreted to mean that the vibration of the first span affects the dynamic response of the second span. In general, it is seen from these figures that the dynamic amplification factors of the hinged-span type bridge are very large in comparison with those of the continuous-span type bridge.

7. CONCLUSIONS

An analytical method for free vertical vibration and dynamic response of suspension bridges, including the effects of shear deformation and rotary inertia, has been developed in this study. The differential equations of motion and the associated boundary conditions are derived by applying Hamilton's principle. The eigenfunctions are divided into three categories by way of taking the eigenvalues as shown in **Table 1**. The dynamic response of suspension bridges under moving loads is solved by the modal analysis method, and the solution is expressed in a closed form. The major conclusions of this investigation are summarized as follows:

(1) It can be concluded from the numerical results of natural frequencies that the effect of the support conditions of the tower cable saddle is comparatively small and is limited to only the first few modes. However, the difference due to the boundary conditions of the siffening girder is considerable. The values of the natural periods of hinged suspension bridges are generally larger than those of continuous suspension bridges.

(2) The effects of shear deformation and rotary inertia on the natural frequencies are very clear for small π and increase with the increasing parameter r. Since the effects of shear deformation and rotary inertia become particularly significant for the higher modes, it is necessary to consider these effects in the dynamic analysis of vertically vibrating suspension bridges.

(3) For the first principal modes, the continuous suspension bridges are very susceptible to shear deformation and rotary inertia in comparison with the hinged suspension bridges.

(4) The hinged suspension bridges produce the bent-angle at the intermediate supports, but the continuous suspension bridges do not produce one. From an engineering standpoint, the continuous suspension bridges have the advantage of good stability for railway vehicles in contrast to the hinged suspension bridges in general use.

(5) The dynamic amplification factors have a tendency to increase as the speed parameter increases and as the parameter r increases. The dynamic effects of the hinged suspension bridges under moving loads are generally large in comparison with those of the continuous suspension

bridges.

(6) The great effects of shear deformation and rotary inertia on dynamic response of suspension bridges under moving loads are observed in the continuous-span type bridge.

The present study has been provided as a basis for a dynamic analysis of the vibration of suspension bridges which take into account the effects of shear deformation and rotary inertia. These effects on the free vibration and dynamic response of suspension bridges under moving loads are investigated by parameters r and π. Within the writer's knowledge, the ranges of parameters r and π in actual suspension bridges are approximately from 0.005–0.03 and 0.1–0.3, respectively. Therefore, it is concluded that the both effects in discussing this problem are impossible to disregard. It is possible also that in this study the shear deformation and rotary inertia are considered separately. The individual effects should be investigated in any future work to determine their characteristics.

8. ACKNOWLEDGMENTS

The writer wishes to thank Professor N. Watanabe of the Hokkaido University for his critical reading of the manuscript and for offering many valuable suggestions. The writer is also grateful to Mr. H. Ohshima of the Honshu-Shikoku Bridge Authority for his provision of technical data on the Innoshima Suspension Bridge. The numerical computations were carried out with the digital computer HITAC M-200H of the Hokkaido University Computing Center. Furthermore, the writer gratefully acknowledges financial support from the Scientific Research Fund (Bountry Research A) of the Ministry of Education.

REFERENCES

1) Bleich, F. et al.: The Mathematical Theory of Vibration in Suspension Bridges, U.S. Gov. Printing Office, Washington, 1950.
2) Hawranek, A. und O. Steinhardt: Theorie und Berechnung der Stahlbrücken, Springer-Verlag, Berlin, 1958.
3) Moppert, H.: Statische und dynamische Berechnung erdverankerter Hängebrücken mit Hilfe von Greenschen Funktionen und Integralgleichungen, Stahlbau-Verlags-GmbH, Köln, 1955.
4) Klöppel, K. und K. H. Lie: Lotrechte Schwingungen von Hängebrücken, Ingenieur-Archiv, Vol. 13, pp. 211～266, 1942.
5) Maeda, Y. et al.: Natural vibration analysis of suspension bridges, Proc. JSCE, No. 262, pp. 13～24, June 1977 (In Japanese).
6) Huang, T. C.: The effect of rotatory inertia and of shear deformation on the frequency and normal mode equations of uniform beams with simple end conditions, J. Appl. Mech., Vol. 28, pp. 579～584, Dec. 1961.
7) Cheng, F. Y.: Vibrations of Timoshenko beams and frameworks, Proc. ASCE, Vol. 96, No. ST 3, pp. 551～571, Mar. 1970.
8) Clough, R. W.: On the importance of higher modes of vibration in the earthquake response of a tall building, Bulletin of the Seismological Society of America, Vol. 45, pp. 289～301, Oct. 1955.
9) Abdel-Ghaffar, A. M. and G. W. Housner: An Analysis of the Dynamic Characteristics of a Suspension Bridge by Ambient Vibration Measurements, EERL 77-01, California Institute of Technology, Pasadena, 1977.
10) Abdel-Ghaffar, A. M. and G. W. Housner: Ambient vibration tests of suspension bridge, Proc. ASCE, Vol. 104, No. EM5, pp. 983～999, Oct. 1978.
11) Abdel-Ghaffar, A. M.: Vertical vibration analysis of suspension bridges, Proc. ASCE, Vol. 106, No. ST10, pp. 2053～2075, Oct. 1980.
12) Vellozzi, J.: Vibration of suspension bridges under moving loads, Proc. ASCE, Vol. 93, No. ST 4, pp. 123～138, Aug. 1967.
13) Hirai, A. and M. Ito: Response of suspension bridges to moving vehicles, Journal of the Faculty of Engineering, University of Tokyo (B), Vol. 29, pp. 1～52, 1967.
14) Ito, M.: Response of suspension bridges to moving vehicles, Proc. JSCE, No. 149, pp. 1～17, Jan. 1968 (In Japanese).
15) Hurty, W. C. and M. F. Rubinstein: Dynamics of Structures, Prentice-Hall, Inc., Englewood Cliffs, N. J., 1964.
16) Cowper, G. R.: The shear coefficient in Timoshenko's beam theory, J. Appl. Mech., Vol. 33, pp. 335～340, June 1966.
17) Hayashikawa, T. and N. Watanabe: Suspension bridge response to moving loads, Proc. ASCE, Vol. 108, No. EM 6, pp. 1051～1066, Dec. 1982.
18) Rayleigh, J. W. S.: The Theory of Sound, Dover Publications, Inc., New York, N. Y., 2nd edition, Vol. 1, pp. 262～265, 1945.
19) Hayashikawa, T. and N. Watanabe: Dynamic behavior of continuous beams with moving loads, Proc. ASCE. Vol. 107, No. EM 1, pp. 229～246, Feb. 1981.
20) Wendroff, B.: Theoretical Numerical Analysis, Academic Press, New York, N. Y., 1966.

(Received August 12, 1982)

土木学会論文報告集 第335号

走行荷重による吊橋の動的応答におけるせん断変形と回転慣性の影響

（林 川 俊 郎）

昭和58年7月

吊橋は長大な支間長を有し，かつ他の橋梁形式と比べて比較的剛性が低いため，風荷重，地震荷重および走行荷重などの動的外力による挙動が工学上問題となることが多い．したがって，この種の橋梁を設計する際には固有振動数および固有振動モードを正確に求めることが必須条件となっている．

従来の吊橋の固有振動解析は静的問題の場合と同様に，簡便性のある線形化撓度理論に基づく計算方法が用いられ，また吊橋の動的設計に広く使用されている．しかし，今までの研究および設計では補剛桁のせん断変形および回転慣性の影響は無視されている．この両者の影響は補剛桁の曲げ変形に比べて比較的小さいということから，また問題の簡単化のため今まで無視されてきた．

一般的に，せん断変形と回転慣性の影響は高次振動モードに対して顕著に現われることが桁およびフレームなどの骨組構造物で知られている．単径間吊橋では1次振動モードが支配的であり，走行荷重による動的応答解析では2，3次までの固有振動モードを知れば実用上十分な応答値を得ることができる．しかし，吊橋の径間数が増えると，その動的応答解析は10数次の高次振動モードまで必要となる．したがって，走行荷重による多径間吊橋の動的応答解析ではせん断変形と回転慣性の影響を無視することはできなくなる．

本研究の第1の目的は，せん断変形と回転慣性を考慮した吊橋の固有振動解析方法を示し，低次から高次の振動モードまで精度よく固有振動数および固有振動モードを求めることである．問題の定式化はTimoshenkoはり理論に従う．吊橋の運動方程式とそれに伴う境界条件式は，Hamilton原理により誘導される．次に，第2の目的は走行荷重による多径間吊橋の動的応答に対する閉じた解を得ることである．また，その動的応答性状におけるせん断変形と回転慣性の影響について調べることである．

最後に，実在吊橋の断面諸元を用いた数値計算例が示される．そこでは，補剛桁の支持条件（ヒンジ形式と連続形式）および塔とケーブルとの結合条件（ローラー結合とヒンジ結合）が吊橋の振動性状に与える影響について比較検討される．吊橋の塔の曲げ変形の影響は低次振動モードに若干現われるが，高次振動モードではほとんどその影響は見受けられない．一方，補剛桁の支持条件による差異は振動モードの次数に限らず顕著に現われる．一般的に，2ヒンジ吊橋の固有周期は連続吊橋のものに比較して大きい値を示す．また，走行荷重による2ヒンジ吊橋の動的影響（動的増加率）は連続吊橋よりも大きいことが示される．さらに，せん断変形と回転慣性の影響は吊橋の鉛直たわみ固有振動性状および動的応答性状において，決して無視できない因子であることがここで指摘される．